Optimizing the Viewing Graph for Structure-from-Motion

Chris Sweeney[1]   Torsten Sattler[2]   Tobias Höllerer[1]   Matthew Turk[1]   Marc Pollefeys[2]

[1]University of California Santa Barbara
{cmsweeney, holl, mturk}@cs.ucsb.edu

[2]Department of Computer Science
ETH Zürich, Switzerland
{sattlert, marc.pollefeys}@inf.ethz.ch

Abstract

The viewing graph represents a set of views that are related by pairwise relative geometries. In the context of Structure-from-Motion (SfM), the viewing graph is the input to the incremental or global estimation pipeline. Much effort has been put towards developing robust algorithms to overcome potentially inaccurate relative geometries in the viewing graph during SfM. In this paper, we take a fundamentally different approach to SfM and instead focus on improving the quality of the viewing graph before applying SfM. Our main contribution is a novel optimization that improves the quality of the relative geometries in the viewing graph by enforcing loop consistency constraints with the epipolar point transfer. We show that this optimization greatly improves the accuracy of relative poses in the viewing graph and removes the need for filtering steps or robust algorithms typically used in global SfM methods. In addition, the optimized viewing graph can be used to efficiently calibrate cameras at scale. We combine our viewing graph optimization and focal length calibration into a global SfM pipeline that is more efficient than existing approaches. To our knowledge, ours is the first global SfM pipeline capable of handling uncalibrated image sets.

1. Introduction

The viewing graph is a fundamental tool in the context of Structure-from-Motion (SfM) [20, 26, 29]. This graph encapsulates the cameras that are to be estimated as vertices and the relative geometries between cameras as edges. SfM algorithms take the relative geometries from the viewing graph as an input and output a reconstruction consisting of camera poses and 3D points. The traditional method for computing a SfM reconstruction is incremental SfM [28, 32] which progressively grows a reconstruction by adding one new view at a time. Incremental SfM requires repeatedly performing nonlinear optimization (*i.e.*, bundle adjustment) as the reconstruction grows in size. As a re-
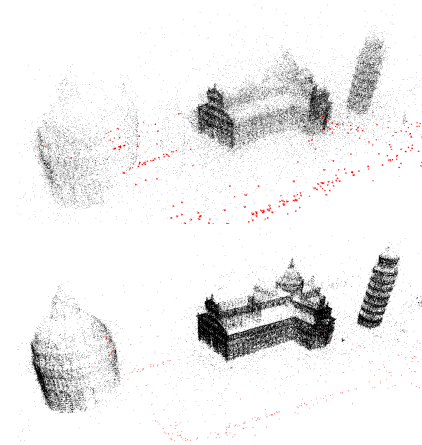

Figure 1. Reconstructions computed from global SfM methods on the Pisa dataset [16]. **Top:** Standard global SfM pipelines [31] struggle to handle image sets with poor calibration or inaccurate relative geometries. **Bottom:** Our method optimizes the relative geometries in the viewing graph to enforce global consistency, resulting in an efficient SfM pipeline that handles calibrated or uncalibrated images.

sult, incremental SfM is able to overcome noise in the viewing graph because errors and inaccuracies from the viewing graph are consistently corrected through bundle adjustment.

Much recent work has focused on so-called "global SfM" techniques that consider all relative poses (*i.e.*, edges in the viewing graph) to simultaneously estimate all camera poses in a single step [3, 11, 12]. These methods operate on calibrated image sets by first estimating the global orientation of all cameras simultaneously [6, 13, 14, 21], then solving for the camera positions simultaneously [3, 16, 22, 31]. Finally, structure is estimated and a global bundle adjustment is applied. Since bundle adjustment is generally the most expensive part of SfM, global SfM methods are generally more efficient and scalable than incremental methods as they only require a single bundle adjustment.

Since global SfM relies on averaging relative rotations and translations, the quality of the input relative poses di-

rectly affects the final reconstruction quality. Various filtering techniques exist [16, 31] to remove outlier edges from the viewing graph; however, it is clear to see that the effectiveness of these methods will decrease when the accuracy of relative geometries in the viewing graph decreases, since it will be more difficult to distinguish noise from outliers. Inaccurate relative geometries are common in the context of SfM from internet photo collections [28] and may arise from a variety of reasons including poor calibration, repeated structures, image noise, and poor or sparse feature matches. Indeed, much effort has been put towards designing robust SfM algorithms that are capable of overcoming potentially inaccurate relative geometries.

In this paper, we approach SfM from a fundamentally different perspective: rather than treating potentially inaccurate two-view geometry as static input to SfM, we instead attempt to recover a consistent viewing graph from a noisy one such that the performance of any SfM method will be improved. In practice, it is unlikely that we are able to recover a perfectly consistent viewing graph; however, we show that enforcing loop consistency in the viewing graph makes estimating structure and motion easier by improving the convergence of current SfM algorithms. As our main contribution, we propose a novel method to optimize the viewing graph and enforce global consistency through loop constraints. We use the epipolar point transfer across triplets in the viewing graph as a geometric error for loop consistency and directly optimize fundamental matrices connecting views. An important contribution of our viewing graph optimization is that it is able to operate on calibrated or uncalibrated datasets, and we present a scalable calibration method for determining focal lengths of uncalibrated cameras (see Section 5).

Our optimization is able to greatly improve the accuracy of relative poses in the viewing graph (see Section 6), and the resulting optimized viewing graph does not require any filtering steps during SfM to remove "bad" relative geometries. This is in contrast to alternative methods [16, 22, 31] which require complex filtering steps throughout camera pose estimation. As a result, we are able to design a simple global SfM pipeline (compared to alternative approaches such as [16, 22, 31]) that is extremely efficient. To our knowledge, this is the first global SfM method that is able to handle uncalibrated image sets. We demonstrate on several large scale datasets that our optimization and simplified SfM pipeline is able to greatly improve the efficiency of large scale SfM while maintaining comparable accuracy.

1.1. Related Work

We will briefly present some of the related works here, and will present other related works throughout the remainder of the paper.

Much previous work has analyzed the viewing graph.

Levi and Werman [20] presented a theoretical analysis of viewing graphs, and provide linear methods for inferring missing edges from a consistent viewing graph given up to 6 views. Rudi *et al*. [26] present a followup to this work by analyzing the solvability of viewing graphs in the context of creating reconstructions. Both of these works, however, only analyze characteristics of consistent viewing graphs.

In contrast, Pillai and Govindu [25] assume they are given a non-consistent viewing graph and present a method that attempts to modify it to form a consistent viewing graph. They iteratively re-estimate pixels locations of observed feature points based on the epipolar point transfer, then use these updated feature points to re-estimate fundamental matrices connecting views. This process is repeated until convergence; however, convergence is not guaranteed and even on the small datasets presented (fewer than 15 images) the method does not converge after 200 iterations.

2. The Viewing Graph

A scene consisting of n views may be represented by a *viewing graph* $\mathcal{G} = \{\mathcal{V}, \mathcal{E}\}$ whose vertices $\mathcal{V}$ correspond to views in the scene and whose edges $\mathcal{E}$ correspond to feature matches and relative geometries between two views, namely the fundamental matrix connecting two views. Specifically, F_{ij} is the fundamental matrix that transfers points in image j to lines in image i. The viewing graph contains information about the relative geometry between views but does nothing to enforce geometric constraints beyond 2-view geometry. For example, there may be triplets (loops of size 3) whose relative geometry is not geometrically feasible when considering all three edges [26, 33]. Ideally, the edges in these loops would be consistent with each other.

Condition 1. *A triplet of fundamental matrices is consistent when they satisfy [15]:*

$$e_{ik}^\top F_{ij} e_{jk} = e_{ij}^\top F_{ik} e_{kj} = e_{ji}^\top F_{jk} e_{ki} = 0 \ , \qquad (1)$$

where e_{ij} is the epipole of F_{ij} corresponding to the image of camera center j in view i and $e_{ij} \neq e_{ik}$ i.e., the non-collinearity condition is satisfied.

Definition 1. *A consistent viewing graph is a viewing graph where all triplets satisfy Condition 1.*

The geometric interpretation of Definition 1 is that the projection of view k's camera center in image i is consistent with the projection of view k's camera center in image j transferred to image i by the fundamental matrix F_{ij}.

Let us now consider the existence of a consistent viewing graph:

Theorem 1. *Given a reconstruction $\mathcal{R} = \{\mathcal{P}, \mathcal{X}\}$ consisting of projection matrices $\mathcal{P}$ and 3D points $\mathcal{X}$, a non-empty set of consistent viewing graphs exists.*

Proof. A consistent viewing graph may be constructed directly from the reconstruction $\mathcal{R}$ by setting each edge $e_C \in \mathcal{E}$ to the fundamental matrix composed from the two corresponding projection matrices [15]. By construction, Condition 1 is satisfied. □

Thus, for every reconstruction $\mathcal{R}$ there exists a consistent viewing graph $\mathcal{G}_C$ that will generate $\mathcal{R}$. Further, it is known that computing a reconstruction from a consistent viewing graph may be done trivially by chaining projection matrices computed directly from the fundamental matrices in the viewing graph [26, 27]. Computing a reconstruction from a non-consistent viewing graph, however, is much more difficult and is the crux of most SfM methods.

3. Creating a Consistent Viewing Graph

Rather than facing the difficult task of computing a reconstruction from a non-consistent viewing graph $\mathcal{G}$, we propose to instead recover a consistent viewing graph $\mathcal{G}_C$ from $\mathcal{G}$ so that computing a reconstruction is simplified [15, 26]. Thus, the goal of this paper is to optimize a noisy, non-consistent viewing graph $\mathcal{G} = \{\mathcal{V}, \mathcal{E}\}$ to recover a consistent viewing graph $\mathcal{G}_C$ that will improve SfM. This requires adjusting the edges $F_{ij} \in \mathcal{E}$ to enforce Condition 1. We propose an optimization scheme that uses a geometric error to enforce loop constraints that attempt to satisfy Condition 1. If we are able to recover a consistent viewing graph then computing a reconstruction is trivial; however, even in the case that we cannot recover a fully consistent viewing graph the accuracy of the relative geometries improves enough that computing structure and motion is greatly simplified (*c.f.* Section 4).

In the remainder of this section we propose an optimization that operates on the viewing graph, enforcing loop consistency with the epipolar point transfer. Our optimization recovers an approximately consistent viewing graph $\mathcal{G}_{OPT}$ that improves the performance of SfM by improving convergence in the estimation process.

3.1. Enforcing Loop Consistency

We now propose a cost function for adjusting $\mathcal{E}$ to enforce triplet consistency in $\mathcal{G}$. While Condition 1 is a sufficient condition for consistency [26], it is an algebraic metric and is significantly under-constrained. Instead, we propose to use the epipolar point transfer to enforce loop consistency. The epipolar point transfer is defined as the intersection of two transfer lines of two views into a third view (*c.f.* Figure 2).

$$\hat{x}_i^{jk} = F_{ij}x_j \times F_{ik}x_k \ , \tag{2}$$

where x_i is the feature point in image i and $\hat{x}_i^{jk}$ is the estimated pixel location of x_i based on the epipolar transfers from views j and k. In the ideal case we will have
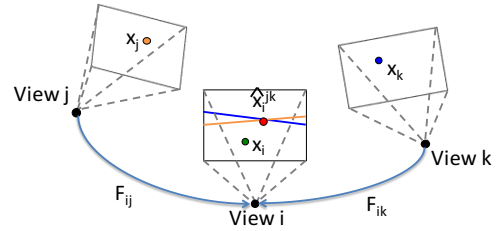

Figure 2. The epipolar point transfer is the intersection of the points x_j and x_k transferred to image i. We enforce loop consistency in the viewing graph by optimizing fundamental matrices such that the distance between the observed point x_i and the epipolar point transfer x_i^{jk} is minimized.

$x_i = \hat{x}_i^{jk}$; however, this is almost never the case in real data because of image noise and outliers in the feature matching process. Instead, we define a cost function based on the epipolar point transfer:

$$C(x)_i^{jk} = ||x_i - \hat{x}_i^{jk}||_2 \ . \tag{3}$$

This cost is a geometric error in terms of pixel distance and has previously been shown to be effective [10, 25]; however, care must be taken to avoid numerical instabilities (see Section 3.4).

3.2. Updating Fundamental Matrices

We seek to adjust fundamental matrix edges $F_{ij} \in \mathcal{E}$ in $\mathcal{G}$ based on Eq. (3). Fundamental matrices are a special class of rank-2 matrices [1]. Thus, updating a fundamental matrix during the nonlinear optimization must be done carefully to ensure that the resulting 3×3 matrix remains a valid fundamental matrix. We use the nonlinear fundamental matrix representation of Bartoli and Sturm [4] to update the fundamental matrices and briefly summarize their method here.

Note that a fundamental matrix F may be decomposed into matrices U, S, and V by singular value decomposition $F = USV^\top$, where U and V are orthonormal matrices and S is a 3×3 diagonal matrix of the form $diag(1, s, 0)$. To update F, we apply a $SO(3)$ rotation to the $O(3)$ matrices U and V, and a simple scalar addition to s.

$$U \leftarrow R_u U \tag{4}$$
$$V \leftarrow R_v V \tag{5}$$
$$s \leftarrow s + \delta_s \tag{6}$$

Since R_u and R_v are $SO(3)$ rotations, they may be represented with the minimal 3 parameters (by Euler angle or angle axis representation), thus requiring 7 parameters total (3 for R_u, 3 for R_v and 1 for δ_s) to update F. Since F has 7 degrees of freedom, this is a minimal parameterization and has been shown to maintain valid fundamental matrices [4].

3.3. Nonlinear Optimization

We create a large nonlinear optimization using the cost function of Eq. (3) and the presented method for updating fundamental matrices. We only optimize edges that are present in triplets $\mathcal{T}$ in the viewing graph:

$$\mathbf{F}^* = \arg\min_F \sum_{t \in \mathcal{T}} \sum_{x \in t} C(x)_i^{jk} + C(x)_j^{ik} + C(x)_k^{ij} \ , \quad (7)$$

where x is a feature track present in the triplet $t = \{i, j, k\}$ and $\mathbf{F}$ is the set of fundamental matrices $F \in \mathcal{E}$. That is, for all triplets, we minimize the epipolar point transfer cost of all feature tracks within the triplet. Although the epipolar point transfer cost function does not require a triplet of fundamental matrices, we found that using triplets greatly improved the rate of convergence. Further, since each camera interacts with other cameras that might not be linked together in a triplet, larger loops are implicitly created.

Finally, it should be noted that the feature points x are treated as constant in Eq. (7) and alternatively could be treated as free parameters that are optimized with the fundamental matrices. We found that additionally optimizing feature points with fundamental matrices resulted in a dramatic decrease in efficiency and did not provide significantly better results.

3.4. Numeric Instabilities

The epipolar point transfer has known degeneracies and numeric instabilities [15]. In particular, any configuration in which the transfer point lies on the trifocal plane of the images i, j, and k will be degenerate and points near this degeneracy are increasingly ill-conditioned. To avoid ill-conditioned points, we do not consider points where the two transfer lines are nearly parallel or when the transfer lines lay near the epipole. The latter scenario can be checked by examining the norm of the transfer line. Since the epipole is in the null space of F_{ij}, the norm of the transfer line will be very small when it is near the epipole.

It should be noted that if the three camera centers are collinear then there is a one-parameter family of planes containing the three cameras and thus the trifocal plane is ambiguous. We explicitly avoid this scenario by removing collinear triplets where the epipoles are equal. In practice, we did not find this to be a limitation since nearly all cameras in real datasets are constrained by at least one non-collinear camera triplet.

4. Estimating Structure and Motion

Given a consistent viewing graph, estimating structure and motion is extremely simple. To see why this is the case, let us consider a consistent and calibrated viewing graph $\mathcal{G}_C$. Since the graph is consistent, this means that the relative rotations in each triplet in $\mathcal{G}_C$ are also consistent (*i.e.*,

---

Algorithm 1 Standard Global SfM Pipeline

1: **procedure** GLOBAL SFM($\mathcal{G} = \{\mathcal{V}, \mathcal{E}\}$, Focal lengths)
2:     Filter $\mathcal{G}$ from loop constraints [8, 22, 33]
3:     Robust orientation estimation [6]
4:     Filter relative poses [16, 22, 31]
5:     Robust Position Estimation [8, 16, 22, 31]
6:     Triangulate 3D points
7:     Bundle Adjustment
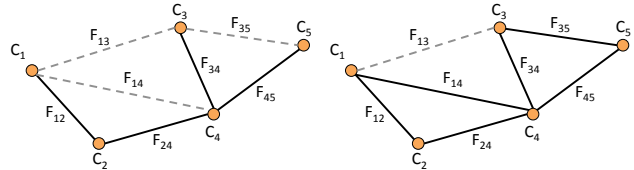8: **end procedure**

Figure 3. In order to reduce size of the viewing graph optimization, we construct a subgraph from the maximum spanning tree (MST). Edges in the MST (left) are shown with thick lines. Edges from the original viewing graph (dashed lines) are then added to the MST if they form a triplet to form $\mathcal{G}'$ (right).

concatenating the relative rotations in a triplet will form a loop: $R_{ij} R_{jk} R_{ki} = I$). The global orientations of each camera may be easily obtained from a random spanning tree [6] or from a linear orientation method [21]. A consistent viewing graph also means that the relative translation directions in $\mathcal{G}_C$ are perfect *i.e.*, $\alpha_{ij} t_{ij} = R_i(c_j - c_i)$. Thus, estimating the camera positions (assuming orientation is known) is equivalent to recovering the baselines α_{ij} between cameras. This pipeline is simpler than alternative global SfM approaches that require many filtering steps and more complex motion estimation algorithms [16, 22, 31] (*c.f.* Algorithm 1).

While our viewing graph optimization is not guaranteed to create a consistent viewing graph, the optimization enforces enough of a consistency constraint that the SfM process can be simplified. In fact, we are able to remove all filtering steps from our SfM pipeline, and are able to further simplify the orientation and position estimation algorithms.

4.1. Viewing Graph Optimization

The viewing graph optimization described in Section 3 has $O(|\mathcal{E}|)$ free parameters, and thus the run time of the nonlinear optimization scales directly with the number of edges. Viewing graphs may contain highly redundant information, and so we would like to reduce the number of edges in the viewing graph so as to reduce the size of the nonlinear optimization. This is similar to the skeletal set selection of Snavely *et al.* [29], whose goal is to find a minimal set of views in the viewing graph that represent the entire scene. Our goal, in contrast, is to find a minimal set of edges that provide sufficient coverage over all views in the viewing

---

Algorithm 2 Our Global SfM Pipeline

1: **procedure** OUR GLOBAL SFM($\mathcal{G} = \{\mathcal{V}, \mathcal{E}\}$)
2:     Choose subgraph $\mathcal{G}'$ (Section 4.1)
3:     Optimize the $\mathcal{G}'$ for consistency (Section 3)
4:     [optional] Calibrate cameras (Section 5)
5:     Estimate camera orientation from Eq. (8)
6:     Estimate camera positions from Eq. (9)
7:     Triangulate 3D points
8:     Bundle Adjustment
9: **end procedure**

---

graph.

Given an input viewing graph $\mathcal{G} = \{\mathcal{V}, \mathcal{E}\}$, we aim to create a subgraph $\mathcal{G}'$ that sufficiently covers the viewing graph with a minimum number of edges. Similar to [9], we first select the maximum spanning tree $\mathcal{G}' = \mathcal{G}_{MST}$ where edge weights are the number of inliers from fundamental matrix estimation between two views then find all edges $\mathcal{E}_T \in \mathcal{E}$ that, if added to $\mathcal{G}'$ would create a triplet in the graph (*i.e.*, a loop of size 3) as show in Figure 3. Among the edges in $\mathcal{E}_T$ we select a set of "good" edges $\mathcal{E}_G$ that have a triplet projection error less than τ (see Appendix A) and add these to the graph. The triplet projection error is an approximate error measurement to determine how close a triplet of fundamental matrices is to being consistent (Condition 1). We repeat this procedure (*i.e.*, $\mathcal{G}' = \mathcal{G}' \cup \mathcal{E}_G$) until every view in the viewing graph participates in at least one triplet, or there are no more "good" edges that can be added.

After we have obtained a representative viewing graph $\mathcal{G}'$, we must choose which feature tracks to use for the optimization. Similar to Crandall *et al.* [7], we use a set cover approach to select a subset of all feature tracks to accelerate optimization. In each image, we create an $N \times N$ grid and choose the minimum number of feature tracks such that all grid cells in all images contain at least one track in the optimization. We have found that choosing spatially distributed feature points helps the viewing graph optimization to converge to a better minimum.

Finally, we use all selected edges and feature tracks to optimize the viewing graph by minimizing Eq. (7) using the Ceres Solver optimization library [2]. We use a Huber loss function to remain robust to outliers from feature matching.

4.2. Estimating Motion

The resulting optimized viewing graph provides accurate fundamental matrices that nearly form a consistent viewing graph (*c.f.* Figure 5). As a result, there is no need for further outlier filtering during the structure and motion estimation. Further, there is no longer a need for robust methods such as [6] or [31]. This simplifies the SfM pipeline from a mathematical standpoint and for implementation purposes. The result is a more efficient pipeline with comparable accuracy to current methods.

Assuming the cameras are calibrated (or calibration is obtained with the method of Section 5), computing the orientations is simple. We solve for orientations by enforcing the relative rotation constraint $R_{ij} = R_j R_i^\top$. Similar to the method of [21], we minimize the cost function

$$\sum_{i,j} ||R_i R_{ij} - R_j||_2 \qquad (8)$$

to solve for camera orientations. Martinec and Pajdla [21] use a linear least squares technique to solve for matrices that minimize Eq. 8; however, this requires the solutions of the linear system to be projected into SO(3) matrices in order to obtain valid rotations. In contrast, we use the angle-axis parameterization (which ensures that all rotations R_i remain on the rotation manifold throughout the optimization[6]) and minimize Eq. (8) with a nonlinear solver. The orientations are initialized by chaining relative rotations from a random spanning tree as is done in the initialization for [6]. This simplified orientations solver is $2 - 4\times$ more efficient than the method of [6] while producing orientations that typically differ less than $1°$ for the datasets in Table 2.

To compute camera positions, we use the same nonlinear position constraint as Wilson and Snavely [31], though our pipeline does not require filtering steps before solving for camera positions. Given a relative translation t_{ij} and a known camera orientation R_i, we use the following constraint to estimate camera centers c_i and c_j:

$$t_{ij} = R_i \frac{(c_j - c_i)}{||c_j - c_i||} \ . \qquad (9)$$

This nonlinear constraint is known to be more stable than other cross-product constraints [3, 11]. We use the Ceres Solver library [2] to solve the nonlinear Eq. (8) and Eq. (9) for recovering camera orientations and positions. After estimating camera poses, we triangulate 3D points and run a single bundle adjustment. Our SfM pipeline is summarized in Algorithm 2.

5. Focal Length Calibration

A current limitation of global SfM methods is that they require relative poses in the form of relative rotations and translations as input. For calibrated image sets, the relative poses may be obtained by decomposing the essential matrix [15]. For uncalibrated cameras, only the fundamental matrix is available between two views. Focal lengths may be obtained from the fundamental matrix in closed form [18] and the resulting essential matrix may be decomposed into relative rotations and translations. The relative rotations and translations obtained through fundamental matrix decomposition, however, are far less accurate compared to when calibration is known (*c.f.* Figure 4) so obtaining accurate
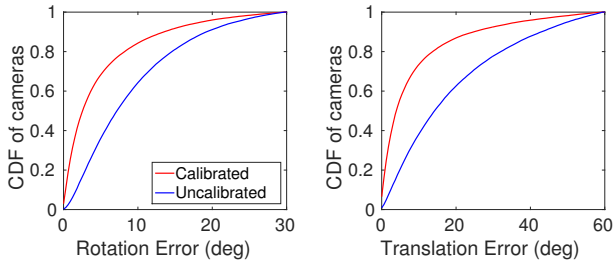
Figure 4. We measured the effect of calibration on relative pose error. When using known calibration (red) the relative rotation and translations are significantly more accurate then when calibration is unknown (blue). For unknown calibrations, we compute relative rotations and translations by decomposing the fundamental matrix.

calibration has a direct effect on the quality of SfM algorithms.

Individually decomposing fundamental matrices from all relative geometries containing a particular camera, however, is not guaranteed to yield a single consistent focal length value. That is, each decomposition of a fundamental matrix containing a particular camera may yield a different focal length value for that camera. Further, the quality of the focal lengths computed from a fundamental matrix is solely dependent on the quality of the fundamental matrix estimation. Focal lengths are not a lie group and so a simple averaging of focal lengths does not give statistically meaningful results [5] and a more meaningful metric is needed to effectively "average" focal lengths. In this section we propose a new calibration method for simultaneously determining the focal lengths of all cameras in a viewing graph using only fundamental matrices as input.

5.1. Focal Length from a Fundamental Matrix

First, let us review a technique for determining focal lengths from a single fundamental matrix. An essential matrix E has the form $t \times R$ for a given relative translation t and rotation R if and only if E is rank 2 with its two non-zero singular values equal [15]. This property may be encapsulated by the scalar invariants of E [17]:

$$C = ||EE^\top||^2 - \frac{1}{2}||E||^4 \ . \qquad (10)$$

For a valid essential matrix E, the cost function C will be 0. Kanatani and Matsunaga [18] show that Eq. (10) may be used to recover the two focal lengths from a fundamental matrix by noting that:

$$E = K'^\top F K \ . \qquad (11)$$

When the focal lengths are unknown, C is a non-negative cost function whose minimum is at 0. By inserting Eq. (11) into Eq. (10), we may solve for the focal length values that minimize C. This may be solved in closed form by noting that the first order partial derivatives $\partial C / \partial f'$ and $\partial C / \partial f$ must also be 0 [18].
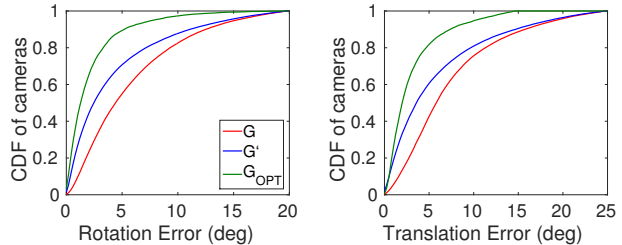

Figure 5. We plot the relative rotation and translation errors of the initial viewing graph $\mathcal{G}$, the subgraph $\mathcal{G}'$ and the viewing graph after optimization $\mathcal{G}_{OPT}$ when executed on the uncalibrated images from the Colosseum dataset [32]. The subgraph $\mathcal{G}'$ has lower relative pose errors than the initial viewing graph and the viewing graph optimization greatly improves the quality of relative poses.

5.2. Focal Lengths from the Viewing Graph

Kanazawa *et al*. [19] extend Eq. (10) to a triplet of fundamental matrices with a simple cost function:

$$C = C(F_{12}) + C(F_{13}) + C(F_{23}) \ . \qquad (12)$$

When image noise is present, this non-negative cost function is no longer guaranteed to have a minimum at $C = 0$; however, minimizing this function is shown to produce good estimations of focal lengths for the triplet [19]. We extend this triplet formulation to operate on an entire viewing graph:

$$\boldsymbol{f}^* = \arg\min \sum_{F \in \mathcal{G}} C(F) \ , \qquad (13)$$

where $\boldsymbol{f}^* = \{f_0, \ldots, f_n\}$ is the set of all focal lengths of all views in the viewing graph $\mathcal{G}$. The focal length values are obtained by minimizing the cost function of Eq. (10) over all fundamental matrices that correspond to edges in the viewing graph. We use an L_1 loss function to minimize the terms of Eq. (13) to maintain robustness to outliers.

The minimization of Eq. (13) can easily be modified to handle viewing graphs with partially known calibration by keeping the known focal lengths constant during the minimization. Similarly, Eq. (13) can be easily modified to handle the case of all cameras sharing the same focal length.

6. Results

We evaluate our algorithm on a number of small to large-scale benchmark datasets consisting of internet photo collections of popular landmarks. All experiments were performed on a 2008 Mac Pro with 2.26 GHz processor and 24 GB of RAM using a single core.

6.1. Viewing Graph Optimization

We demonstrate the effectiveness of our viewing graph optimization by examining the relative rotation and translation errors of the viewing graph compared to a refer-
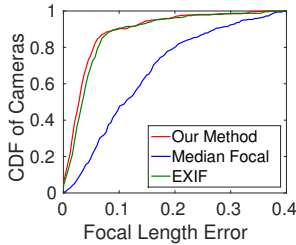
Figure 6. We show the accuracy of calibration methods on the Pisa dataset [16] and show the focal length error $|f - f_{gt}|/f_{gt}$ compared to ground truth focal lengths obtained from a reconstruction from VisualSfM [32]. Our method is at least as accurate as using EXIF, and is significantly more accurate than using the median focal lengths obtained from fundamental matrix decomposition.

Table 3. Running time in seconds for the 1DSfM [31] experiment. T_{BA} and T_Σ denote the final bundle adjustment time and the total running times for each reconstruction method. T_{OPT} is the time our method takes for the viewing graph optimization. Our method is 2 to 9 times faster than alternative global SfM methods.

Name	1DSfM [31]		LUD [24]		Cui *et al.* [8]		Our Pipeline		
	T_{BA}	T_Σ	T_{BA}	T_Σ	T_{BA}	T_Σ	T_{OPT}	T_{BA}	T_Σ
Piccadilly	2425	3483	-	-	-	-	310	702	1246
Union Square	340	452	-	-	-	-	98	102	243
Roman Forum	1245	1457	-	-	-	-	284	847	1232
Vienna Cathedral	2837	3139	208	1467	717	959	139	422	607
Piazza del Popolo	191	249	31	162	93	144	12	78	101
NYC Library	392	468	54	200	48	90	14	83	154
Alamo	752	910	133	750	362	621	18	129	198
Metropolis	201	244	-	-	-	-	27	94	161
Yorkminster	777	899	148	297	63	108	13	71	102
Montreal N.D.	1135	1249	167	553	226	351	61	133	266
Tower of London	606	648	86	228	121	221	92	246	391
Ellis Island	139	171	-	-	64	95	12	14	33
Notre Dame	1445	1599	126	1047	793	1159	59	161	247

ence reconstruction computed by VisualSFM[1]. The relative translation error is the angular distance (in degrees) between R_{ij} from the viewing graph and $R_j R_i^\top$ composed from the reference reconstruction. Similarly, the relative translation error is the angular distance (in degrees) between the unit-norm vectors t_{ij} from the viewing graph and $\overline{t_{ij}} = (c_j - c_i)/||c_j - c_i||$ created from camera position c_j and c_i from the reference reconstruction. That is, $t_{err} = acos(t_{ij}^\top \overline{t_{ij}})$ is the translation error in degrees. We compare the relative pose errors on three different viewing graphs: the initial input viewing graph $\mathcal{G}$, the unoptimized subgraph $\mathcal{G}'$ (see Section 4.1), and the viewing graph after the viewing graph optimization $\mathcal{G}_{OPT}$.

The relative pose errors from the Colosseum dataset[32] are shown in Figure 5. The subgraph $\mathcal{G}'$ is effective in removing some of the inaccurate edges in $\mathcal{G}$; however, it is clear to see that our viewing graph optimization significantly improves the accuracy of relative poses. The mean relative rotation error on the Colosseum dataset is reduced from $8.3°$ in $\mathcal{G}$ to $7.5°$ in $\mathcal{G}'$ to $2.49°$ in $\mathcal{G}_{OPT}$. The mean relative translation error is reduced from $22.6°$ in $\mathcal{G}$ to $19.3°$ in $\mathcal{G}'$ to $3.29°$ in $\mathcal{G}_{OPT}$. We include results for the Pisa and Trevi datasets [16] in the supplemental material[2].

6.2. Focal Length Calibration

To determine the accuracy of our calibration method, we used images from the Pisa and Trevi datasets [16] that contain EXIF focal lengths and compare our calibration to reference focal lengths that were obtained from a reference reconstruction generated with VisualSfM [32] after bundle adjustment of the internal and external camera parameters. We compare our method to using EXIF data for calibration as well as the median focal length. The median focal length is obtained by decomposing all fundamental matrices connected to a view and taking the median of the focal lengths

---

[1]The reconstructions obtained with VisualSFM [32] are not meant to serve as ground truth but merely a reference for a good reconstruction.

[2]The supplemental material can be found on the author's website

obtained from the decompositions.

We plot the accuracy of the focal lengths obtained with each method in Figure 6. For simplicity, we only plot the results from the Pisa dataset; however, the results from the Trevi dataset were similar. For both datasets our calibration method converged in less than 10 seconds. Our method is at least as accurate as using focal length values from EXIF data. The accuracy stems from the use of many two-view constraints to estimate the focal length. EXIF values can be accurate but have the potential to be inaccurate if the image has been resized or cropped. Using the median focal length is very inaccurate and is not sufficient for use in a SfM pipeline.

6.3. Structure-from-Motion

We ran our pipeline on the small-scale dataset of [30] and the large-scale datasets of [31] to measure the performance and feasibility of our method on real data. We compare our SfM pipeline to several alternative global SfM pipelines, and the results are summarized in Tables 1, 2, and 3.

Table 2 shows that our method is approximately up 2 to 10 times more efficient than alternative methods, while maintaining comparble accuracy to the state-of-the-art. The increase in efficiency is a direct result of our simplified SfM pipeline (see Section 4) that is able to efficiently utilize the high quality relative poses obtained from the optimized viewing graph. The statistical pose averaging (*c.f*. Eq. (8) and Eq. (9)) converges to a high quality result very quickly because our optimized viewing graph is extremely accurate (*c.f*. Figure 5). Visualizations of the reconstructed datasets are included in the supplemental material.

7. Conclusion

In this paper, we have presented a new approach to large-scale SfM. Rather than focusing on creating potentially complex algorithms to overcome noise and outliers in the reconstruction process, we propose an optimization that

Table 1. We evaluate several SfM pipelines on the Strecha MVS datasets [30]. Our method shows excellent accuracy while remaining extremely efficient. Timing results of Cui *et al.* [8] were not available.

	Accuracy (mm)					Time (s)			
Name	VSFM [32]	Olsson [23]	Cui *et al.* [8]	Moulon [22]	Ours	VSFM [32]	Olsson [23]	Moulon [22]	Ours
FountainP11	7.6	**2.2**	2.5	2.5	2.4	**3**	133	5	4.5
EntryP10	63.0	6.9	-	5.9	**5.7**	**3**	88	5	3.8
HerzJesuP8	19.3	3.9	-	**3.5**	3.5	2	34	2	**1.9**
HerzJesuP25	22.4	5.7	**5.0**	5.3	5.3	12	221	10	**9.3**
CastleP19	258	76.2	-	**25.6**	38.2	9	99	6	**5.7**
CastleP30	522	66.8	**21.2**	21.9	32.4	18	317	14	**11.6**

Table 2. We compare results of several global SfM pipelines on the large-scale 1DSfM dataset [31]. We show the number of cameras reconstructed N_C and the median position error approximately in meters $\widetilde{x}$. For our method, $\widetilde{x}$ indicates position errors before bundle adjustment, and $\widetilde{x}_{BA}$ are the errors after bundle adjustment. Our method produces accurate camera poses before bundle adjustment and has comparable accuracy to alternative methods after bundle adjustment.

		1DSfM [31]		LUD [24]		Cui *et al.* [8]		Our Pipeline		
Name	N_c	N_c	$\widetilde{x}$	N_c	$\widetilde{x}$	N_c	$\widetilde{x}$	N_c	$\widetilde{x}$	$\widetilde{x}_{BA}$
Piccadilly	2152	1956	0.7	-	-	-	-	1928	5.2	1.0
Union Square	789	710	3.4	-	-	-	-	701	4.5	2.1
Roman Forum	1084	989	0.2	-	-	-	-	966	6.8	0.7
Vienna Cathedral	836	770	0.4	750	5.4	578	3.5	771	6.7	0.6
Piazza del Popolo	328	308	2.2	305	1.5	298	2.6	302	2.9	1.8
NYC Library	332	295	0.4	320	2.0	288	1.4	294	2.8	0.4
Alamo	577	529	0.3	547	0.4	500	0.6	533	1.4	0.4
Metropolis	341	291	0.5	-	-	-	-	272	8.7	0.4
Yorkminster	437	401	0.1	404	2.7	333	3.7	409	3.9	0.3
Montreal N.D.	450	427	0.4	433	0.5	426	0.8	416	2.0	0.3
Tower of London	572	414	1.0	425	4.7	393	4.4	409	9.3	0.9
Ellis Island	227	214	0.3	-	-	211	3.1	203	3.7	0.5
Notre Dame	553	507	1.9	536	0.3	539	0.3	501	9.4	1.2

corrects the viewing graph and enforces global consistency via loop constraints before applying SfM. We demonstrated that this optimization improves the quality of relative geometries in the viewing graph and removes the need for complex filtering steps as part of the SfM pipeline. Our viewing graph optimization works on calibrated or uncalibrated image sets and we provide a new method for calibrating cameras from a set of fundamental matrices. We incorporated the viewing graph optimization and focal length calibration into a global SfM pipeline that is intuitive to understand and easy to implement, and showed that this pipeline achieves greater efficiency and comparable accuracy to the current state-of-the-art methods. For future work we plan to examine the guarantees we can make (if any) on the "consistency" of the viewing graph we obtain from the viewing graph optimization. Additionally, it would be interesting to see if our method may be applied for global SfM on projective reconstructions.

A. Triplet Projection Error

We define here the triplet projection error used in Section 4.1. Given three views, i, j, and k, and the corresponding fundamental matrices F_{ij}, F_{ik}, and F_{jk}, Sinha *et al.* [27] compute a consistent triplet of fundamental matrices. We use their technique to define a triplet projection error that measures the consistency of a triplet of fundamental matrices. We will briefly summarize the method here.

First, projection matrices for views i and j and k are constructed from the fundamental matrices

$$P_i = [I|0] \tag{14}$$
$$P_j = [[e_{ji}]_\times F_{ij}|e_{ji}] \tag{15}$$
$$P_k = [[e_{ki}]_\times F_{ik}|0] + e_{ki}v^\top \tag{16}$$

where v is an unknown 4-vector. Recall from [15] that a fundamental matrix may be constructed from the projection matrices of the two views it connects:

$$\overline{F}_{jk}^\top = [e_{kj}]_\times P_k P_j^+. \tag{17}$$

$\overline{F}_{jk}$ is linear in v and all possible solutions for $\overline{F}_{jk}$ span the subspace of possible fundamental matrices that will form a consistent triplet as defined in Condition (1) [27]. We solve for v that yields $\overline{F}_{jk}$ closest to F_{jk}. We define the triplet projection error as the difference of $\overline{F}_{jk}$ and F_{jk} by Frobenius norm:

$$Err_{ijk} = ||\overline{F}_{jk} - F_{jk}|| \ . \tag{18}$$

References

[1] S. Agarwal, H. l. Lee, B. Sturmfels, and R. R. Thomas. Certifying the existence of epipolar matrices. *arXiv preprint arXiv:1407.5367*, 2014.

[2] S. Agarwal, K. Mierle, and Others. Ceres solver. `http://ceres-solver.org`.

[3] M. Arie-Nachimson, S. Z. Kovalsky, I. Kemelmacher-Shlizerman, A. Singer, and R. Basri. Global motion estimation from point matches. In *International Conference on 3D Imaging, Modeling, Processing, Visualization and Transmission (3DIMPVT)*, pages 81–88. IEEE, 2012.

[4] A. Bartoli and P. Sturm. Nonlinear estimation of the fundamental matrix with minimal parameters. *IEEE Transactions on Pattern Analysis and Machine Intelligence*, 26(3):426–432, March 2004.

[5] M. Bujnak, Z. Kukelova, and T. Pajdla. 3d reconstruction from image collections with a single known focal length. In *Proceedings of the IEEE International Conference on Computer Vision (ICCV)*, pages 1803–1810. IEEE, 2009.

[6] A. Chatterjee and V. M. Govindu. Efficient and robust large-scale rotation averaging. In *Proceedings of the IEEE International Conference on Computer Vision (ICCV)*, pages 521–528. IEEE, 2013.

[7] D. Crandall, A. Owens, N. Snavely, and D. P. Huttenlocher. Discrete-continuous optimization for large-scale structure from motion. In *Proceedings of the IEEE Conference on Computer Vision and Pattern Recognition (CVPR)*, 2011.

[8] Z. Cui, N. Jiang, and P. Tan. Linear global translation estimation from feature tracks. In *Proceedings of the The British Machine Vision Conference (BMVC)*, 2015.

[9] O. Enqvist, F. Kahl, and C. Olsson. Non-sequential structure from motion. In *Computer Vision Workshops of the IEEE International Conference on Computer Vision (ICCV)*, pages 264–271. IEEE, 2011.

[10] A. Goldstein and R. Fattal. Video stabilization using epipolar geometry. *ACM Transactions on Graphics (TOG)*, 31(5):126, 2012.

[11] V. M. Govindu. Combining two-view constraints for motion estimation. In *Proceedings of the IEEE Conference on Computer Vision and Pattern Recognition (CVPR)*, volume 2, pages II–218. IEEE, 2001.

[12] V. M. Govindu. Robustness in motion averaging. In *The Asian Conference on Computer Vision*, pages 457–466. Springer, 2006.

[13] R. Hartley, K. Aftab, and J. Trumpf. L1 rotation averaging using the weiszfeld algorithm. In *Proceedings of the IEEE Conference on Computer Vision and Pattern Recognition (CVPR)*, pages 3041–3048. IEEE, 2011.

[14] R. Hartley, J. Trumpf, Y. Dai, and H. Li. Rotation averaging. *International Journal of Computer Vision*, 103(3):267–305, 2013.

[15] R. Hartley and A. Zisserman. *Multiple view geometry in computer vision*. Cambridge university press, 2003.

[16] N. Jiang, Z. Cui, and P. Tan. A global linear method for camera pose registration. In *Proceedings of the IEEE International Conference on Computer Vision (ICCV)*, pages 481–488. IEEE, 2013.

[17] K. Kanatani. *Group-theoretical methods in image understanding*, volume 2. springer-Verlag New York, 1990.

[18] K. Kanatani and C. Matsunaga. Closed-form expression for focal lengths from the fundamental matrix. In *Proceedings of the Asian Conference on Computer Vision*, volume 1, pages 128–133, 2000.

[19] Y. Kanazawa, Y. Sugaya, and K. Kanatani. Decomposing three fundamental matrices for initializing 3-d reconstruction from three views. *IPSJ Transactions on Computer Vision and Applications*, 6:120–131, 2014.

[20] N. Levi and M. Werman. The viewing graph. In *Proceedings of the IEEE Conference on Computer Vision and Pattern Recognition (CVPR)*, volume 1, pages I–518. IEEE, 2003.

[21] D. Martinec and T. Pajdla. Robust rotation and translation estimation in multiview reconstruction. In *Proceedings of the IEEE Conference on Computer Vision and Pattern Recognition (CVPR)*, pages 1–8, June 2007.

[22] P. Moulon, P. Monasse, and R. Marlet. Global fusion of relative motions for robust, accurate and scalable structure from motion. In *Proceedings of the IEEE International Conference on Computer Vision (ICCV)*. IEEE, 2013.

[23] C. Olsson and O. Enqvist. Stable structure from motion for unordered image collections. In *Image Analysis*, pages 524–535. Springer, 2011.

[24] O. Ozyesil and A. Singer. Robust camera location estimation by convex programming. In *The IEEE Conference on Computer Vision and Pattern Recognition (CVPR)*, June 2015.

[25] J. K. Pillai. Consistent averaging of multi-camera epipolar geometries. Master's thesis, India Institute of Science, 2008.

[26] A. Rudi, M. Pizzoli, and F. Pirri. Linear solvability in the viewing graph. In *Proceedings of the Asian Conference on Computer Vision*, pages 369–381. Springer, 2011.

[27] S. N. Sinha, M. Pollefeys, and L. McMillan. Camera network calibration from dynamic silhouettes. In *Proceedings of the IEEE Conference on Computer Vision and Pattern Recognition (CVPR)*, volume 1, pages I–195. IEEE, 2004.

[28] N. Snavely, S. M. Seitz, and R. Szeliski. Photo tourism: exploring photo collections in 3d. In *ACM transactions on graphics (TOG)*, volume 25, pages 835–846. ACM, 2006.

[29] N. Snavely, S. M. Seitz, and R. Szeliski. Skeletal graphs for efficient structure from motion. In *Proceedings of the IEEE Conference on Computer Vision and Pattern Recognition (CVPR)*, volume 1, page 2, 2008.

[30] C. Strecha, W. von Hansen, L. V. Gool, P. Fua, and U. Thoennessen. On benchmarking camera calibration and multi-view stereo for high resolution imagery. In *Computer Vision and Pattern Recognition, 2008. CVPR 2008. IEEE Conference on*, pages 1–8. IEEE, 2008.

[31] K. Wilson and N. Snavely. Robust global translations with 1dsfm. In *Proceedings of the European Conference on Computer Vision*, pages 61–75. Springer, 2014.

[32] C. Wu. Towards linear-time incremental structure from motion. In *Proceedings of the International Conference on 3D Vision*, pages 127–134. IEEE, 2013.

[33] C. Zach, M. Klopschitz, and M. Pollefeys. Disambiguating visual relations using loop constraints. In *Proceedings of the IEEE Conference on Computer Vision and Pattern Recognition (CVPR)*, pages 1426–1433. IEEE, 2010.